YIELDING IN THE ISOTROPIC COMPRESSION OF PORTO SILTY SAND

MIGUEL FERREIRA AMARAL, SARA RIOS and ANTÓNIO VIANA DA FONSECA

about the authors

Miguel Ferreira Amaral
University of Porto,
Portugal
E-mail: mfamaral@fe.up.pt

Sara Rios
University of Porto,
Portugal
E-mail: dec06004@fe.up.pt

António Viana da Fonseca
University of Porto,
Portugal
E-mail: viana@fe.up.pt

Abstract

The yielding locus of a well-graded silty sand was analysed by means of isotropic compression tests and scanning electron microscopy (SEM). The tests were performed with precise instrumentation, for internal and external strain measurements, and shear-wave velocity measurements by means of bender elements. Finally, aiming at an accurate evaluation of the yield stress, four different methods were applied – two quite well know and the other two being innovative – leading to interesting conclusions.

Keywords

silty sand, yield point, isotropic compression, high pressure, seismic waves

1 INTRODUCTION

Modelling the behaviour of a soil, rock or concrete due any stress path, necessarily requires a yield-locus assumption [1] – a point on a curve if that is the object of the analysis – that separates the elastic from the elasto-plastic region. This point indicates the instant at which any stress increment causes irreversible strains that may arise in granular soils from particle crushing or other processes associated with the increase in the compressibility [2,3,4]. However, the beginning of particle crushing is usually gradual; therefore, it is usually difficult to define a clear elastic limit due to an initial load [5]. During reloading and unloading, the soil shows a stiffer behaviour as the particles remain broken [5].

Since the very early years of soil mechanics, researchers created criteria and formulated models in order to explain the concept of yielding in materials [3,6,7]. This paper focuses on the yielding phenomena of a well-graded silty sand subjected to isotropic compression, leading to a definition of practical criteria to evaluate the yield point of a soil submitted to a specific compression test and makes a comparison between them. The isotropic yield pressure can be obtained in the laboratory through the Normal Compression Line (NCL) and Swelling Line (SL) [8], obtained by triaxial isotropic compression tests. Among the most used methods for a yield-point evaluation are [9], [10], [11] and [12]. Other methods were identified based on the plastic work [3]. Later, [13] estimated this parameter using bender-elements testing, having a reference in the constitutive model proposed by [14].

2 EXPERIMENTAL PROGRAM

The experimental program comprised two, isotropic, high-pressure, compression tests over samples moulded with two different void ratios. In these tests a very complete instrumentation was used, including shear-wave velocity (V_S) measurements. Scanning electron microscope (SEM) analyses were also performed for the tested samples.

2.1 SOIL DESCRIPTION

In this study, a unique soil was used: a silty sand resulting from the residual soil generated in the weathering of Porto granite [15,16], recoiled in the University of Porto Experimental Site. These soils are found extensively in the north and central regions of Portugal and are usually

classified as a SM (silty sand) in the Unified Classification System, being very well graded with about 30% of fines. The grain size distribution (Fig. 1) reflects an effective diameter (D_{50}) of 0.25mm, and the uniformity and curvature coefficients are 113 and 2.7, respectively. For the laboratory tests presented here the soil was used in remoulded conditions.

This soil, with values of the liquid limit equal to 34% and a plastic limit of 31%, is considered non-plastic. The maximum dry unit weight obtained in the modified Proctor test is 18.55kN/m³ and the optimum water content is 13.1%(Fig. 2). The particle-specific density (G) is 2.72 and a mineralogical analysis demonstrated that larger grains are essentially quartz, while the smaller are predominantly kaolinitic, with small portions of mica (as will be seen below in Fig. 4).
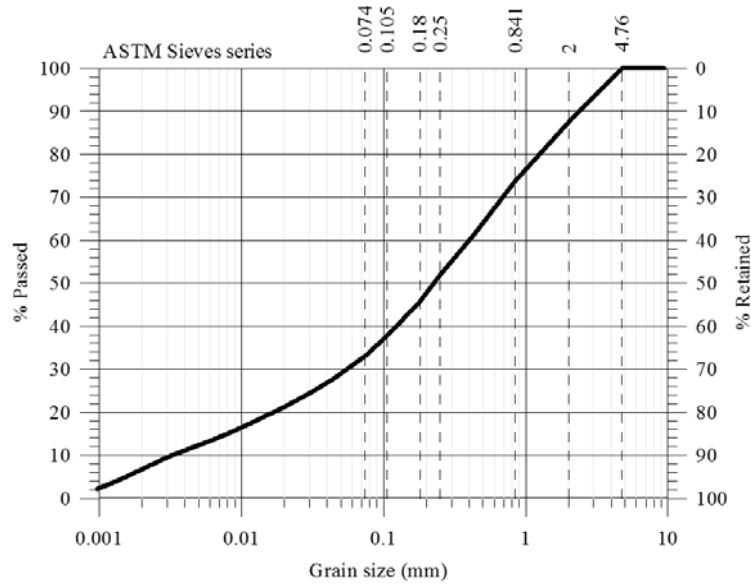

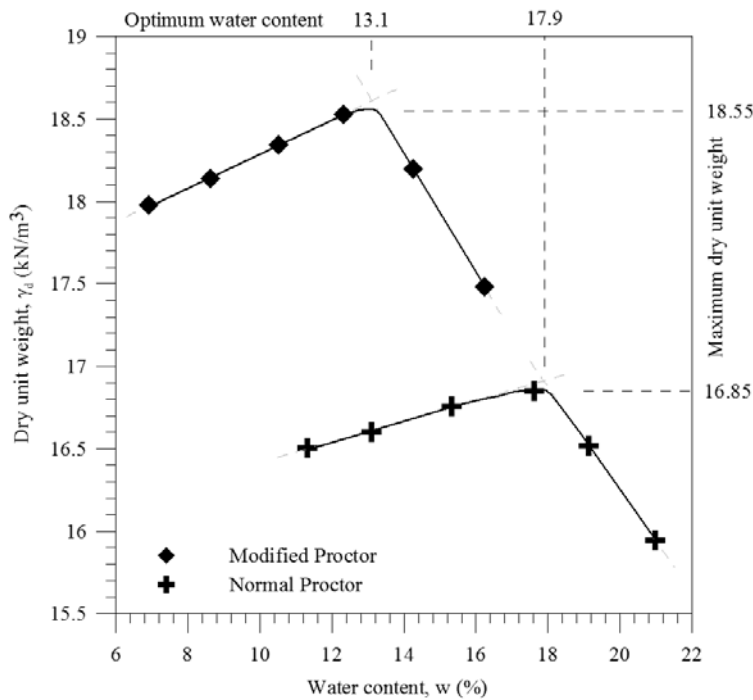**Figure 1**. Porto silty sand grain-size distribution.

Figure 2. Normal and Modified Proctor test of the Porto silty sand.

2.2 SAMPLE PREPARATION

The moulding procedure consisted of a mixture of the right quantities of dry soil and water in order to obtain the desired void ratio and water content. Specimens were statically compacted in a cylindrical mould with a 50mm diameter and around 100mm in length, in two different void ratios (e_i=0.60 and e_i=0.76). After determining the hygroscopic water content of the air dried soil, it was possible to identify the necessary amount of water (distilled water was used) to add to the mixture in order to reach the reference water content of 12%.

The total volume of the mixture was divided into three equal portions and the compaction was made in three layers on a lubricated compacter. After the compaction of one layer, its surface was slightly scarified for better interpenetration with the subsequent layer. At the end of the compaction, the specimens were removed from the mould, measured, weighed, and quickly placed in the tri-axial cell in order to avoid any loss of water. The mass, diameter and length were measured with accuracies of 0.01g and 0.02mm, respectively. The water content was calculated from two small samples of the remaining mixture before compaction.

The samples suitability for testing was defined by the following tolerances:

– Dry Unit Weight (γ_{di}) within ± 1% of target value,
– Water Content (w_i) within ± 1% of the target value,
– Diameter (ϕ_i) within ± 0.5mm,
– Height (H_i) within ± 1mm.

3 METHODS

3.1 EQUIPMENT

The tests were performed in a Hoek-type, high-pressure, tri-axial cell in a room with temperature and humidity control, which were kept in around 20±1°C and 99±1%, respectively. A hollow piston connects the cell fluid between the top and the radial confinement, allowing isotropic compression tests with $\sigma_1 = \sigma_3$.

High-precision instrumentation was used: 2 high-pressure LVDT's to monitor the internal axial strains, 1 high-pressure shear gauge to measure the internal radial deformation, 1 external axial LVDT, 2 GDS® water pressure/volume controllers connected to the specimen's top and bottom – allowing two draining borders – for back-pressure application, pore-pressure measurement and volume-change control, and 1 GDS® silicone oil

pressure/volume controller for the cell pressure. At the top and bottom of the sample porous discs were placed, from which a pair of University-of-Bristol-type connection bender elements protruded [17]. These transducers were used to measure the shear-wave velocity (V_S) during the isotropic compression tests.

Finally, a Field-Emission Scanning Electron Microscope was used to obtain micrographs of the tested samples, i.e., before and after being submitted to very high isotropic pressures.

3.2 TEST PROCEDURES

Immediately after being removed from the mould the sample was accurately measured and then, small holes for the bender elements' insertion and coupling had to be introduced at the top and bottom ends of the sample. This procedure did not take more than 10 minutes and therefore considerable moisture losses were not expected. The specimen was then weighed again ($m_{i,2}$), and so the dry mass of soil lost on the bender elements' holes ($m_{d,L}$) is given by equation (1), relating the difference between the sample mass before and after the holes with the compaction water content (w_i).

$$m_{d,L} = \frac{m_{i,1} - m_{i,2}}{1 + w_i} \qquad (1)$$

The acquisition system was connected just after the conclusion of specimens' installation in the tri-axial cell. A valve connected to the cell was opened, beginning the flow of silicone oil into the cell. At the end of this transference the high-pressure tri-axial cell was sealed.

Small pressures were then applied to the sample to ensure the desired water percolation: 10kPa of cell pressure (CP) and 10kPa of back pressure at the bottom end (BP), with the top of the sample connected by an opened valve to atmospheric pressure.

After the percolation of the total volume of water (200ml) the saturation stage begins, keeping a mean effective stress (p') equal to 10kPa.

$$p' = \frac{\sigma'_1 + 2\sigma'_3}{3} \qquad (2)$$

The saturation is automatically controlled by the three pressure/volume controllers programmed to increment their pressures at a rate of 0.1kPa/s, starting simultaneously. The increase of the pressure finished when CP and BP reached values of 1010kPa and 1000kPa, respectively; after which the pressures were kept constant until the cell

and pore volumes, as well as all the acquired deformations, presented a variation lower than the random noise.

Once the saturation stage ended, the isotropic consolidation stage could be initialised, applying constant-rate $\partial p'$=0.5kPa/s cell-pressure increments, while the back pressure remained equal to 1000kPa. The consolidation was performed in stages, stopping the pressure increment at specific consolidation pressures, which allowed strain stabilization and very accurate seismic-wave measurements. During each consolidation step the Skempton parameter (B) was measured (see table 2):

$$B = \frac{\partial u}{\partial p'} \qquad (3)$$

The necessary increase in the pore pressure, for that purpose, was achieved, so preventing for a short period the water transfer into the BP GDSs (avoiding water-volumes changes, the BP naturally increased). The consolidation went up to 19MPa of effective confining pressure. At the end of each test, the specimens were again measured: final mass ($m_{f,2}$), final dimensions (H_f and ϕ_f) and, final water content (w_f) computed after drying the specimens. For the real final medium's density calculation (ρ_f) it is necessary to correct $m_{f,2}$ from the $m_{d,L}$ deduced from the soil mass lost on the bender elements' coupling holes. The corrected mass ($m_{f,1}$) is given by,

$$m_{f,1} = m_{f,2} + m_{d,L} \times \left(1 + w_f\right) \qquad (4)$$

Then ρ_f is given by,

$$\rho_f = \frac{4 \times m_{f,1}}{\varphi_f^2 \times \pi \times H_f} \qquad (5)$$

The test results were considered suitable if the ratio between the final and initial dry masses was within certain values, as follows,

$$0.975 < \frac{m_{f,1}}{1 + w_f} \times \frac{1 + w_i}{m_{i,1}} < 1.025 \qquad (6)$$

3.3 TEST CORRECTIONS

Table 1 presents the main measurements reported above at the beginning and at the end of the high-pressure isotropic tests, from which the geotechnical parameters presented in this paper were derived. The initial and final volumes (V_i and V_f, respectively) were computed using H_i, ϕ_i, H_f and ϕ_f. The specimens' nomenclature arises from the soil origin and their initial void ratios.

RSS means Residual Soil Soft (e_i=0.76) and RSD means Residual Soil Dense (e_i=0.60).

Table 1. Main parameters measured for the initial and final test conditions.

Specimen	w_i (%)	w_f (%)	$m_{i,1}$ (g)	$m_{f,1}$ (g)	V_i (cm^3)	V_f (cm^3)
RSS	12.21	19.23	353.78	356.16	204.06	166.53
RSD	12.36	17.93	390.68	411.16	204.64	170.21

It is not a novelty that the specimens submitted to a p' increase, suffer a volume reduction. Factors that could cause any strains (such as temperature, relative humidity or BP) were kept constant. Hence it can be assumed that this volume reduction only depends on the p' increase.

In this study, particularly in the bender elements' analysis, it was strictly necessary to estimate the tip-to-tip length between the bender elements ($H_{p'}$) and an average specimen medium's density ($\rho_{p'}$) for each step of the consolidation stage. These quantities also depend on the updated values of the water content ($w_{p'}$), mass ($m_{p'}$), external/internal axial strain ($\varepsilon_{a,p'}$) and volumetric strain ($\varepsilon_{V,p'}$), which is given by $\varepsilon_{a,p'}$ and the internal radial strain ($\varepsilon_{r,p'}$) according to equation (7). The volumetric deformation was either calculated with the external axial strain for seismic-wave measurements or with an internal axial deformation for the void-ratio calculation, in order to account for external effects like bedding errors,

$$\varepsilon_{V,p'} = 2 \times \varepsilon_{r,p'} + \varepsilon_{a,p'} \qquad (7)$$

It is well known that volume adjustments caused by the membrane and the tri-axial cell sealing efforts are smaller for more compacted specimens ([15] and [18]). Therefore, $H_{p'}$ and $\rho_{p'}$ were predicted, taking into account final measurements such as H_f, V_f and w_f, as they represent values for more compacted conditions.

The bender elements had a 4.0mm length, which means $H_{p'}$ can be expressed by equation (8). External instrumentation was used for the axial strain because it refers to the real distance between the bender elements.

$$H_{p'} = \frac{H_f}{1 - \varepsilon_{a,f}} \times \left(1 - \varepsilon_{a,p'}\right) - 2 \times 4.0 (mm) \qquad (8)$$

where $\varepsilon_{a,f}$ is the final external axial strain.

For the updated medium's density determining,

$$\rho_{p'} = \frac{m_{p'}}{V_{p'}} \qquad (9)$$

it is necessary to calculate the updated volume ($V_{p'}$),

$$V_{p'} = \frac{V_f}{1 - \varepsilon_{V,f}} \times \left(1 - \varepsilon_{V,p'}\right) \qquad (10)$$

where $\varepsilon_{V,f}$ is the final volumetric strain given by the acquisition system.

In saturated conditions the updated mass ($m_{p'}$) is directly related with $w_{p'}$ and it may be estimated by,

$$m_{p'} = \frac{m_{f,1}}{1 + w_f} \times \left(1 + w_{p'}\right) \qquad (11)$$

where $w_{p'}$ is calculated as follows,

$$w_{p'} = \left(w_f \times \frac{m_{f,1}}{1 + w_f} + \Delta m_{BP}\right) \times \frac{1 + w_f}{m_{f,1}} \qquad (12)$$

where Δm_{BP} is the mass of the transferred water between each consolidation step.

Finally, the updated specimen medium's density is,

$$\rho_{p'} = \frac{\dfrac{m_{f,1}}{1 + w_f} \times \left[1 + \left(w_f \times \dfrac{m_{f,1}}{1 + w_f} + \Delta m_{BP}\right) \times \dfrac{1 + w_f}{m_{f,1}}\right]}{\dfrac{V_f}{1 - \varepsilon_{V,f}} \times \left(1 - \varepsilon_{V,p'}\right)} \qquad (13)$$

$\varepsilon_{a,f}$ is referred to as final external/internal axial strain because of its implications. When the seismic waves are analysed, the mean of the propagation is the specimens' total length. Thus, the external axial strains should be used. When the purpose is solely to investigate the void-ratio variation, the strains should be taken into account without external effects such as the bedding errors. Thus, the internal axial deformation is used.

4 ISOTROPIC COMPRESSION CURVES

The void-ratio variation is a very sensitive parameter, especially when analysing tri-axial test results. In isotropic tests, good reliability of the initial void ratio is of crucial importance as the relative position of some isotropic curves with respect to the others is controlled by this initial void ratio. On the other hand, being a parameter that can be obtained from different test measurements, it can be treated as a control variable.

During the tests, the specimen's updated void ratio ($e_{p'}$) was calculated by three independent methods given by equations (14) to (16). For this physical parameter estimation only the internal deformations were taken into account.

$$S \times e_{p'} = G \times w_{p'} \iff e_{p'} = \frac{G \times w_{p'}}{S} \qquad (14)$$

where $S \approx 1$ is the saturation degree

$$-\varepsilon_{V,p'} = \frac{e_i - e_{p'}}{1 + e_i} \iff e_{p'} = e_i + \varepsilon_{V,p'}\left(1 + e_i\right) \qquad (15)$$

where e_i is the initial void ratio

$$\rho_{p'} = \rho_S \times \frac{1 + w_{p'}}{1 + e_{p'}} \iff e_{p'} = \rho_S \times \frac{1 + w_{p'}}{\rho_{p'}} - 1 \qquad (16)$$

where ρ_S=2720 kg/m^3 is the particle density of the soil grains.

Fig. 3 (on next page) shows the results of the high-pressure isotropic compression tests for both specimens. The plotted $e_{p'}$ values were computed by averaging all $e_{p'}$ given by equations (14) to (16).

A logarithmic regression was applied to the two line segments of each curve in order to obtain the compression and recompression indexes (C_c and C_r). The obtained values are presented in Fig. 3. It is clear from these results that both curves tend to converge to a unique normal compression line, typical behaviour of a "non-transitional" material [19] expressed in equation (17).

$$e = -0.103\ln\left(p'\right) + 1.25 \qquad (17)$$

Even though the soil involved in these tests can be situated between clean sands and clays, non-significant transitional behaviour [20] was observed in the isotropic compression results and a single NCL was clearly defined. Since it is expected that only gap graded soils can exhibit transitional behaviour, as reported by [19], the very wide grain size distribution curve of this soil might be the reason for not exhibiting such a transitional behaviour.

5 MICROSCOPY

SEM micrographs were taken on a part of the specimens after being tested under high-pressure isotropic compression, and air dried. In Fig. 4 one of those micrographs is shown as an example. The SEM analysis also included the mineralogical composition of some points for particle identification. Being a very well graded soil with around 30% of particles less than 0.075 mm (ASTM sieve No. 200), the bigger particles are all involved by the fine matrix, i.e., with kaolinite giving rise to the texture observed in Fig. 4. However, this very thin layer of clay covering the grains prevents the correct identification of some particles.
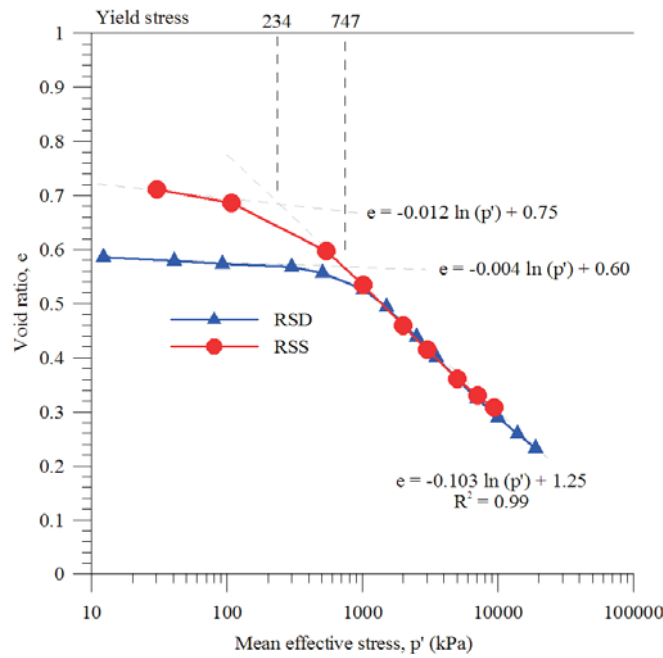
Figure 3. Normal and Modified Proctor test of the Porto silty sand.

In general, the yielding in granular materials is related to particle breakage or associated processes, as stated by several authors [5,21]. However, the amount of breakage is related to the type of grains and the stress level. Sometimes only the weaker grains break, while the strong grains like quartz remain intact [22].

The authors believe that, in this case, the yielding is not related to significant particle breakage (at least of strong quartz grains), but mostly due to the degradation in quartz connections through the kaolinite particles or the bending of micas. Some clear fractures are observed, like the one exhibited in Fig. 4, but they should result from a particle rearrangement with some fissures in the fine matrix of the soil.
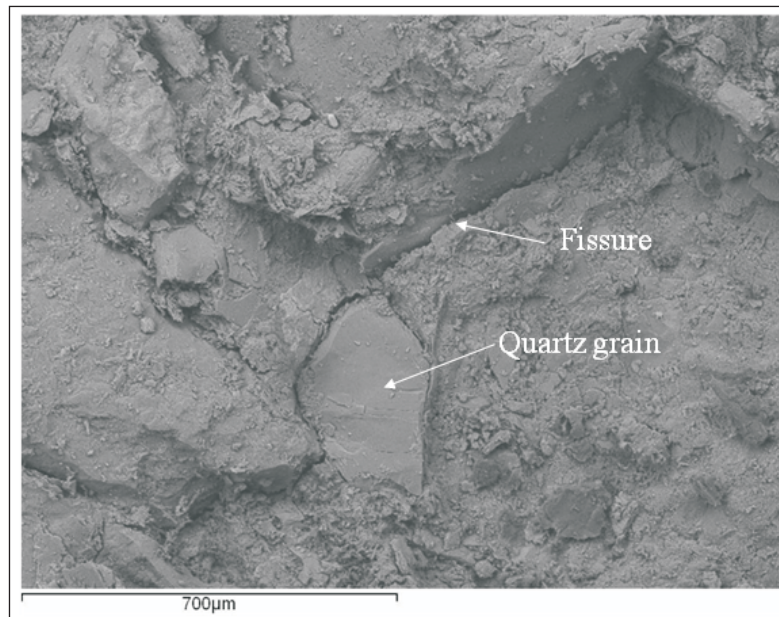

Figure 4. SEM photo of Porto silty sand after a saturated isotropic compression.

As relative movements between the quartz fragments were observed, the yield point and the void-ratio reduction may possibly be a sum of the particle breakage and a pure, non-particle-destructive rearrangement (converging to some qualitative indications referred to by [21]).

6 SEISMIC-WAVE MEASUREMENTS

6.1 INTRODUCTION

Bender elements – introduced in soil mechanics by [23] – are familiar in advanced geotechnical laboratory practices and growing in popularity all over the world. However, nowadays – although changing of the interpretation methods – bender elements are often used in laboratories in order to determine the simple dynamic properties of geomaterials [24,25,26,27,28], in particular the shear-wave velocity (V_S).

According to [29] V_S is related to the dynamic shear modulus (G_0) with the following expression,

$$V_S = \sqrt{\frac{G_0}{\rho_{p'}}} \qquad (18)$$

where $\rho_{p'}$ is the updated medium's density during the process described in equation 12.

6.2 TEST PROCEDURES

The seismic-wave measurements presented herein were only performed with S-waves transmitted vertically and horizontally polarized (V_{Svh}). As both specimens were tested under isotropic stress conditions, it is reasonable to assume that the results provided by a single axis are representative of the three principal directions of inertia. Nevertheless, the sensitivity for the object of this study, i.e., the identification of reliable criteria for yielding identification, is fairly independent of the directions of this transmission/polarization.

Before the tests the bender elements were placed in contact, leading to an approximately 2.0μs delay following the calibration standard procedures [16,30,31]. Fig. 5 illustrates the used connections scheme.

The shear-wave velocities were computed by dividing the tip-to-tip distance between the bender elements ($H_{p'}$), calculated using equation (8) from the external axial measurements, and the shear-wave propagation time (t_s). For the dynamic shear modulus calculation (G_0) the medium's density ($\rho_{p'}$) was derived from equation (13), which was based on external measurements in order to have a global average value of the medium's density for the specimen. Due to border effects, the top and bottom of the sample is often less rigid than the central part, this is why the internal instrumentation is usually placed in
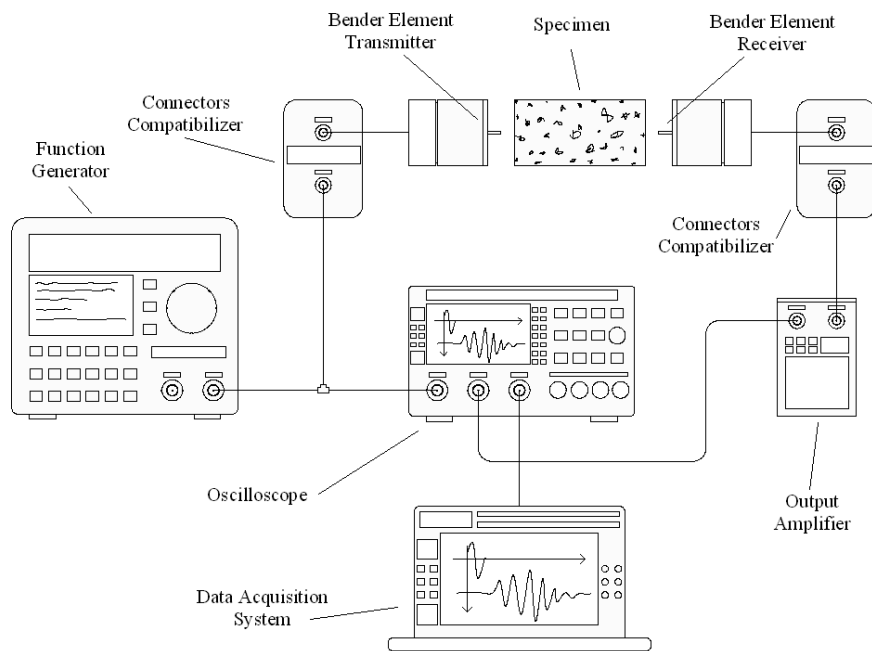

Figure 5. Schematic seismic-wave measurement connections.

that zone. As the wave propagates through the entire height of the sample, an average value of the medium's density was needed, and therefore, the use of external axial deformation and radial deformation for the $\varepsilon_{V,p'}$ computation was considered more appropriate. A simple analysis of the first arrival of the waves was performed based on the time-domain interpretation. As the saturated conditions usually promote fewer amplified signals, to improve the quality of the first arrival a square pulse was used instead of the commonly used sinusoidal pulse [30].

In all the specimens it was observed that the square wave showed more amplified first-arrival results than the sinusoidal ones (e.g., Fig. 6). For some sinusoidal frequencies (Sin. 50 kHz) the S-wave could only be iden- tified further after the square wave's arrival, leading to a significant underestimation of V_S and, consequently, G_0. These observations are in agreement with the numeri- cal simulations of [30]. Based on this assumption, the square pulse was elected as the one that gave the more appropriate results.

6.3 SEISMIC-WAVE RESULTS

The seismic-wave measurements were performed in the consolidation stages after the stabilisation of the internal and external measurements. The following stress stages were considered for each sample: in soft sample (RSS) 8 stages were used at mean effective stresses of 100, 500, 1000, 2000, 3000, 5000, 7000 and 9300 (kPa); in the denser sample (RSD) waves were measured at 100,

300, 500, 1000, 1500, 2500, 3500, 5000, 7000, 10000 and 14000 (kPa) of p' totalising 11 stages.

Figs. 7 and 8 show, for both samples, the shear wave's first arrival in each stress stage.

The results show that the shear wave first arrivals not only tend to be quicker, but they also seem to be more energized with an increase in the effective isotropic stresses, p'. As table 2 testifies, the observed reduction in propagation time also means an increase in the shear- wave velocity, in spite of the progressive decrease in the tip-to-tip distance with the applied load. The results of the Skempton B parameter varying with p' are also presented in table 2, showing an increase in the satura- tion degree with the stress level, as was expected.

Table 2. V_S and B values as a function of p'.

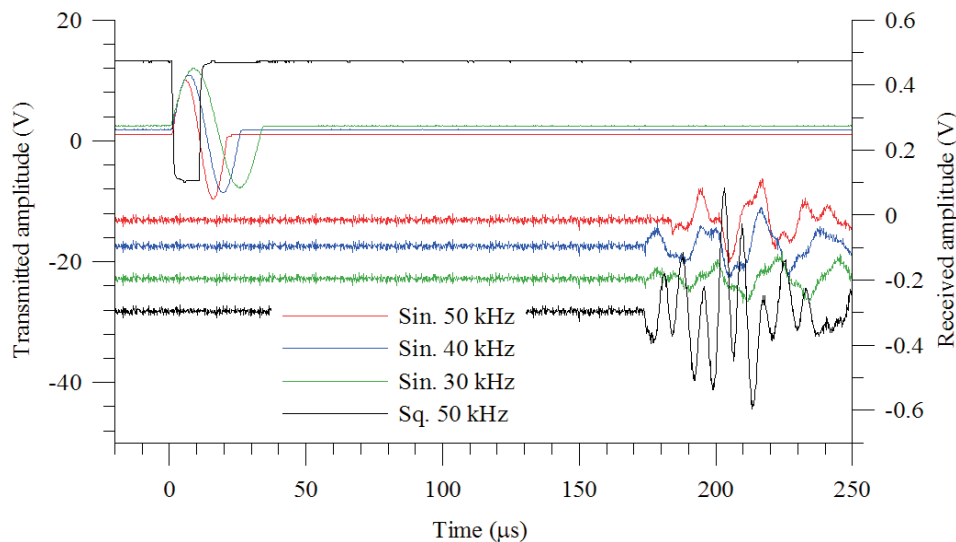|	RSD			RSS	
p' (kPa)	V_S (m/s)	B (%)	p' (kPa)	V_S (m/s)	B (%)
100	495	76	100	488	82
300	496	77	500	483	83
500	496	79	1000	487	84
1000	497	79	2000	491	84
1500	500	80	3000	495	85
2500	504	82	5000	495	87
3500	505	84	7000	497	89
5000	509	85	9300	498	89
7000	509	87			
10000	508	89			
14000	507	91			

Figure 6. Sinusoidal and square-wave impulses: this last one has a higher amplified first-arrival sign.
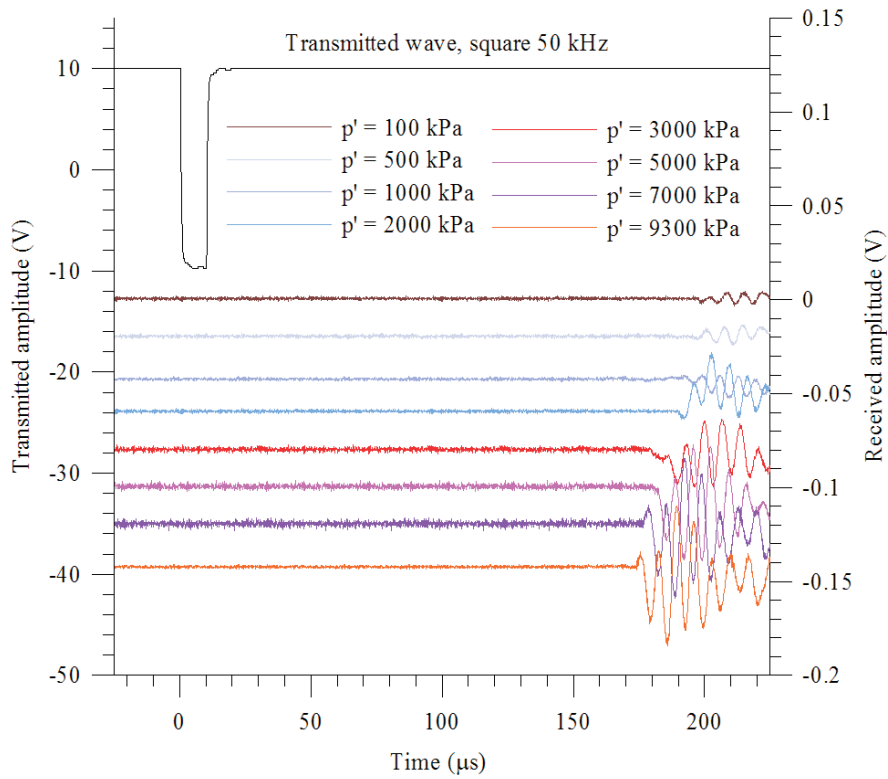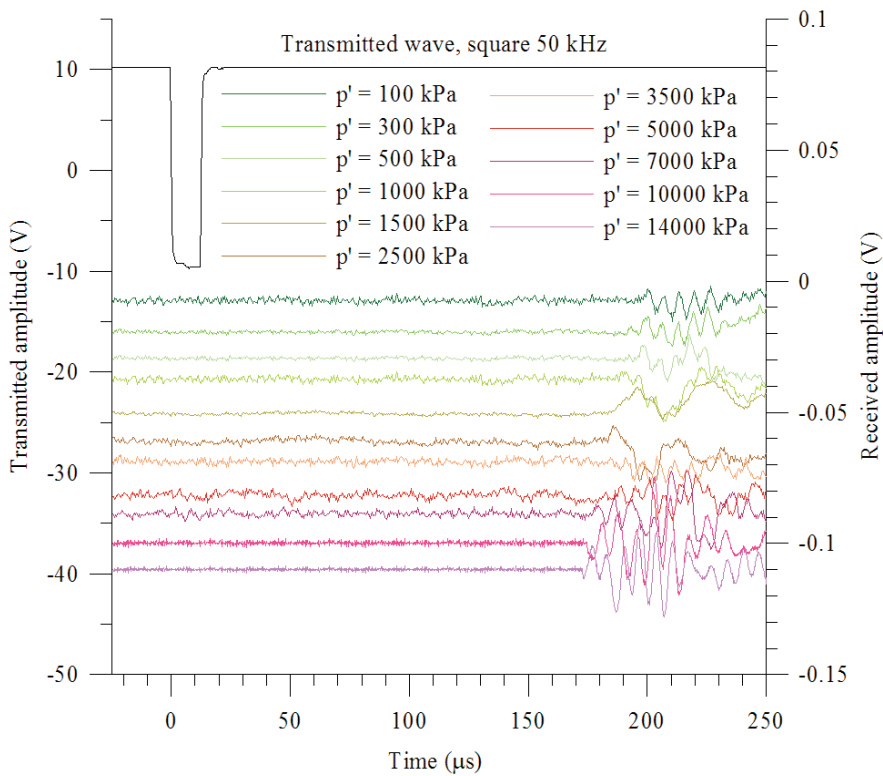
Figure 7. RSS first arrivals for each stress stage.

Figure 8. RSD first arrivals for each stress stage.

7 YIELD STRESS EVALUATION

7.1 INTRODUCTION

One of the aims of this research work was to study and evaluate the yield point of a specific type of geomaterial. Four distinct criteria were applied in order to have an accurate evaluation of this locus. Two of them are some of the most used criteria in soil mechanics; the other two represent an innovative variation of other known criteria.

In this paper – aiming at consistency among criteria – the considered yield point was the p' value of the interception point of two line segments. The first criterion takes into account the elastic and elasto-plastic work ($W_{p'}$) made by the specimens, in the sense that more plastic work means more plastic deformation, which characterises yielding.

The second criterion (G_0 criterion) is based on the maximum shear modulus. According to [13], yielding corresponds to a maximum of the dynamic shear modulus during the loading process, associated with the inflexion of its increase due to the evolution of the pressure towards a consistent drop due to plastic work, allowing the identification of the yield stress.

The third criterion is the most usual, relying on the void-ratio evolution. Finally, the fourth criterion expresses almost the same, as it uses the water-content evolution, which is the outflow of the voids' water. In fact, in saturated conditions the void ratio can be expressed through the water content once there is no air inside the specimen.

For all the criteria it was considered that there were two distinct regions of behaviour: the first one is defined by the predominance of elastic strains (ES), and the second is characterized mostly by its elasto-plastic strains (EPS). Also, for all the criteria, these two regions were defined by straight or logarithmic lines represented by their equations, which involve their slopes and a constant.

7.2 WORK CRITERIA

According to [3], the plastic work (W) in isotropic compression is calculated according to equation (19).

$$W = \int \sigma_3 . d\varepsilon_V \qquad (19)$$

where,

ε_v represents the plastic volumetric strains during isotropic loading.

Normalising that work with respect to volume, the following equation can be used,

$$W_{p'} = p' \times \varepsilon_{V,p'} \qquad (20)$$

where,

$W_{p'}$ is the normalized work (J/m^3);

$\varepsilon_{V,p'}$ is the plastic volumetric strains that change with the stress level.

In Fig. 9, the total work per volume defined as the product of the total volumetric strains (derived from equation (7)) by the mean effective stress is plotted against this last, i.e., p'. The elastic strains are taken into account, defining a tangent line at the beginning of the curve corresponding to the elastic part. Another line, representing a linear regression of the last aligned points intersects the first, giving rise to the yield point.

As it is not plotted on a logarithmic scale, a correct ES definition demands a zoom of the graph to provide details of the elastic part being considered.

The interceptions between ES and EPS lead to mean effective stress yield points of 833kPa and 315kPa for the specimens RSD and RSS, respectively.

7.3 G₀ CRITERIA

This criterion consists of plotting the results from the maximum shear modulus G_0 against p' using a logarithmic scale, as expressed in Fig. 10. According to [14] there are three different yield points distinguishing the zones with different behaviour. These three yield locus concepts should be separated by the coefficients proposed by [14], being Y1 and Y2 applied by [13] for the present study. However, the results in Fig. 10 demonstrate that the Y1 and Y2 location is impossible. The authors believe that those coefficients have values that are too close, enough not to be distinguished by a high-pressure test on this soil.

As was performed in Section 7.2, for Fig. 9, a regression of the two line segments was applied. Once again, computing the ES and EPS interception it is possible to conclude the yielding of 753kPa and 333kPa for the specimens RSD and RSS, respectively.
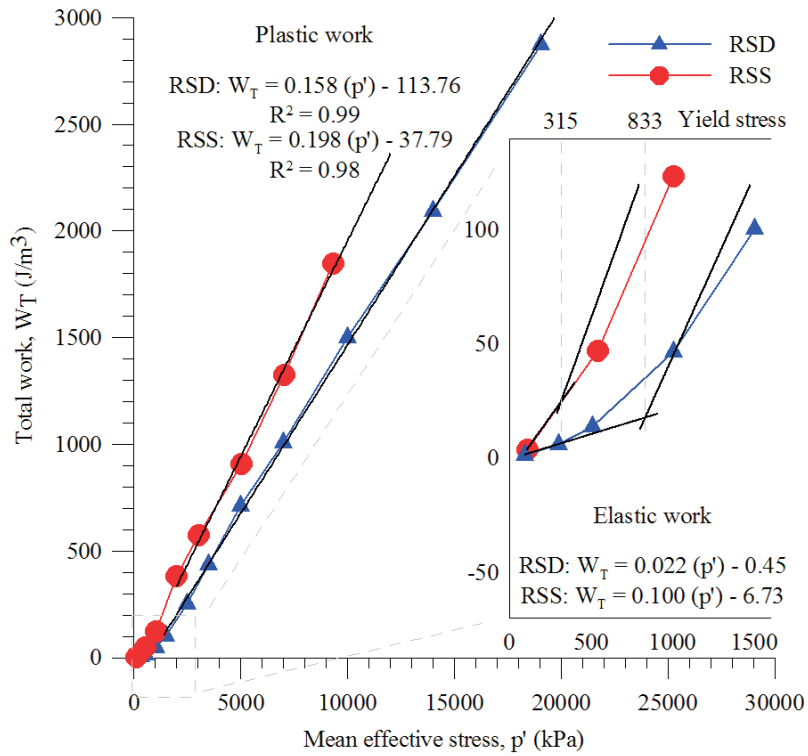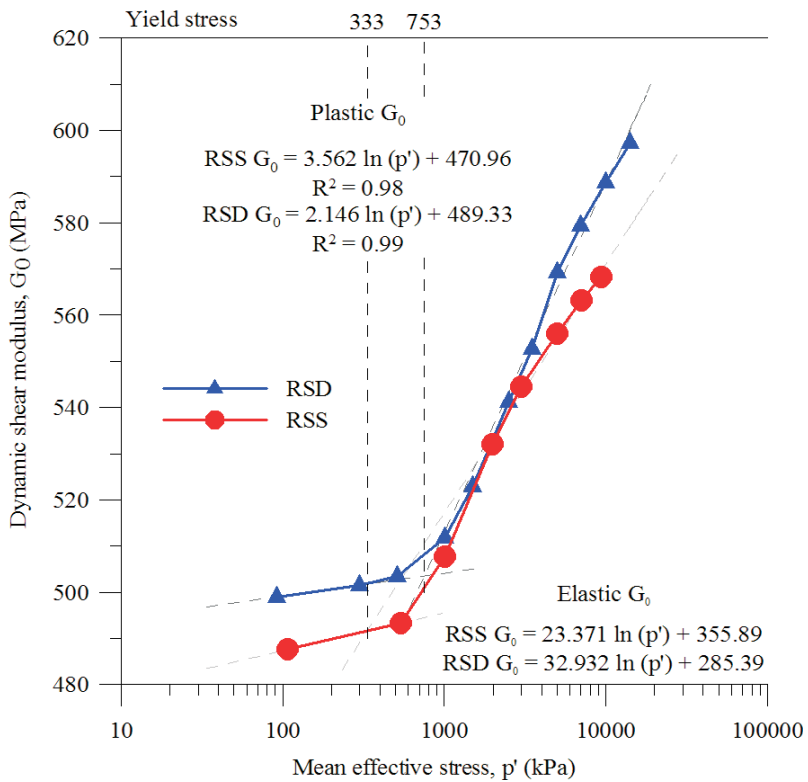
Figure 9. Total work criteria.
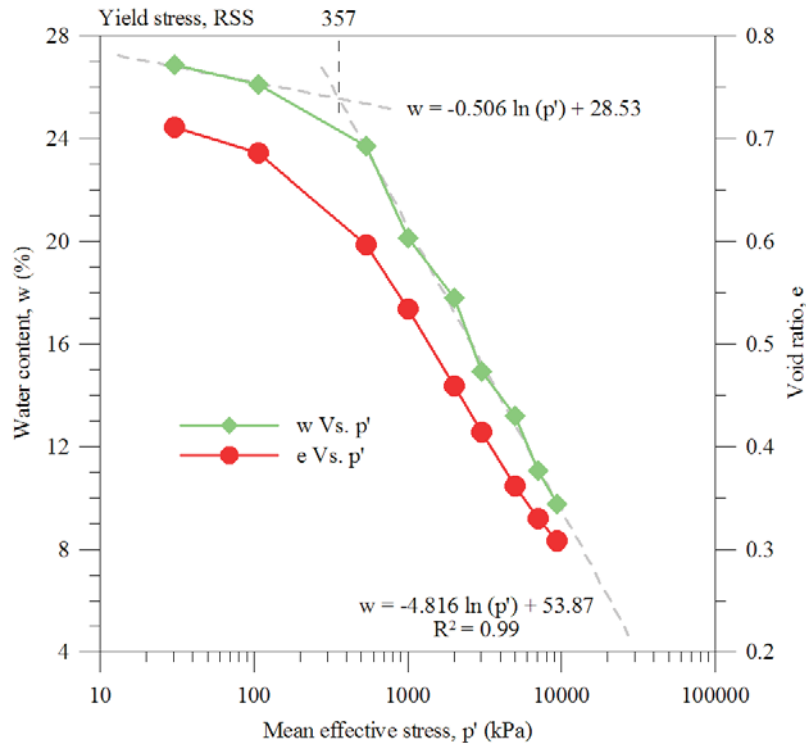

Figure 10. Dynamic shear modulus criterion.

Figure 11. $w_{p'}$ and $e_{p'}$ consolidation variation in the RSD specimen.
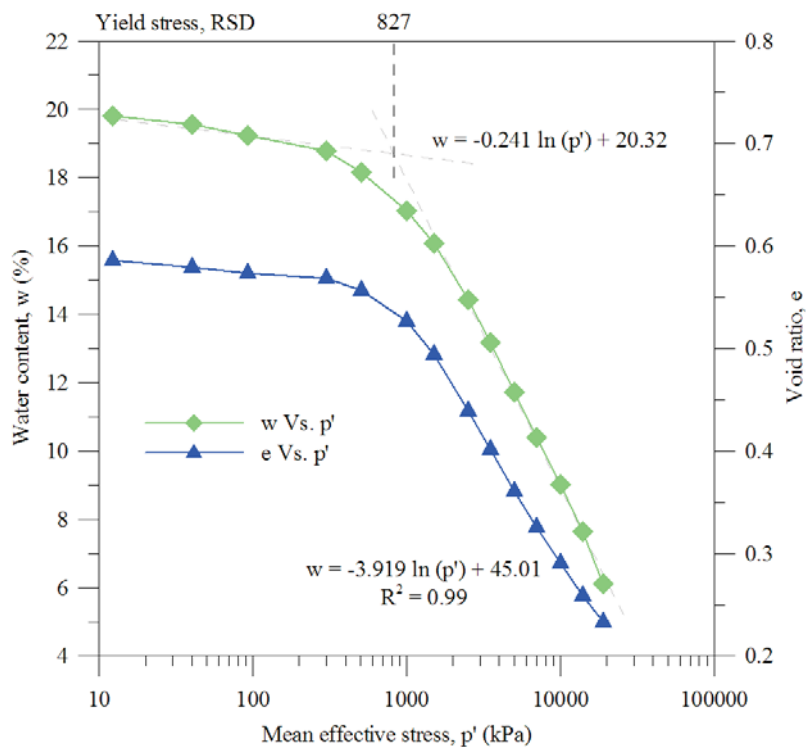

Figure 12. $w_{p'}$ and $e_{p'}$ consolidation variation in the RSS specimen.

7.4 VOID-RATIO AND WATER-CONTENT CRITERIA

As reported above, the third and fourth criteria are similar and thus, plotting $e_{p'}$ against p' should lead to very similar yield-point values than $w_{p'}$ against p' plotting, both on a logarithmic scale.

The isotropic compression curves are presented in Fig. 3, allowing a definition of the two line segments ES and EPS, the interception of which provided the following yielding points: 747kPa and 234kPa, for RSD and RSS, respectively.

According to [32], there is an exact relationship between the specimen's void water volume ($w_{p'}$) and the consolidation pressure. Thus, $w_{p'}$ plotting – in saturated cases – against p', should provide very similar results to $e_{p'}$ vs. p'. In Figs. 11 and 12 the curves of $w_{p'}$ and $e_{p'}$ against p' are plotted together, indicating similar yield points.

The interception of EP and EPS for the water-content curves gave rise to yield-point values of 827kPa and 357kPa for RSD and RSS, respectively. Not only are these values very similar to the void-ratio procedure, but also the graphical trend seems to be very consistent.

7.5 YIELD-STRESS VALUE COMPARISON

The four presented criteria proved to be appropriate in the yield-point evaluation (table 3). Although all the criteria show similar results, the ordinary $e_{p'}$ vs. p' plot showed better consistency in the ES and EPS characterization. However, this paper proved that for simple saturated specimens it is possible to define a yield point using a less rigorous method relating only to the mean effective stress and the water content. This fact allows models, in which the yield-stress definition is a primary concern, not to allow the possibility of simulating it very accurately; these are time-consuming and expensive tests. It was not possible to apply the [14] model, but the results of G_0 proved to be in agreement with the other criteria, defining a very consistent yield point.

Table 3. Results provided by the four yield-point computing criteria (kPa).

Specimen	$w_{p'}$	$e_{p'}$	$W_{p'}$	G_0
RSD	827	742	833	753
RSS	357	218	315	333

CONCLUSIONS

The results provided by this paper lead the authors to the conclusion that yielding is a very sensitive parameter. For a good estimation of yield it is also necessary to use very-high-resolution equipment and very precise instrumentation.

Isotropic compression tests performed at very high pressures over samples moulded at two different void ratios showed that a unique normal compression line could be obtained. These tests were conducted together with seismic-wave measurements and SEM micrographs. The results show that yielding of the well-graded silty sand is not related to a significant particle breakage, but mainly due to fractures in the fine matrix and the bending of micas. Four methods were developed for the yield-stress evaluation, which proved to be quite consistent, giving rise to similar results in spite of the high sensitivity of this parameter.

ACKNOWLEDGMENTS

REFERENCES

[1] Mortara, G. (2008). A new yield and failure criterion for geomaterials. *Géotechnique*, Vol. 58, No. 2, pp. 125-132.

[2] Vesic, A.S., Clough, G.W. (1968). Behavior of granular materials under high stresses. *J. of Soil Mech. & Found. Div.*, Vol. 94, No. SM 3, pp. 661-688.

[3] Lade, P. V. (1977). Elasto-plastic stress-strain theory for cohesionless soil with curved yield surfaces. *Int. J. for Solids Struct.*, Vol. 13, No. 11, pp. 1019-1035.

[4] Konrad, J.M. (1998). Sand state from cone penetrometer tests: a framework considering grain crushing stress. *Géotechnique*, Vol. 48, No. 2, pp. 201-215.

[5] Coop, M.R. (1990). The mechanics of uncemented carbonate sands. *Géotechnique*, Vol. 40, No. 4, pp. 607-626.

[6] Matsuoka, H., Nakai, T. (1974). Stress-deformation and strength characteristics of soil under three different principal stresses. *Proc. Jpn. Soc. of Civ. Eng.*, Vol. 232, pp. 59-70.

[7] van Eekelen, H.A.M. (1980). Isotropic yield surface in three dimensions for use in soil mechanics. *Int. J. Numer. Anal. Methods Geomech.*, Vol 4, No. 1, pp. 89-101.

[8] Taylor, D.W. (1948). Fundamentals of soil mechanics. New York, John Wiley & Sons.

[9] Casagrande, A. (1936). The determination of the pre-consolidation load and its partial significance. *Proc. 1st Int. Conf. On Soil Mech. & Found. Engin.*, Cambridge, Vol. 3, pp. 60-64.

[10] Burmister, D. (1951). The application of controlled test methods in consolidation testing. *Proc. 54th Annu. Meet. of the ASTM, Symp. on Consol. Test. of Soils,* pp. 83-98. (Spec. Tech. Pub., 126).

[11] Schmertmann, J.H. (1955). The undisturbed consolidation behaviour of clay. *Trans. Soc. Civ. Eng.*, Vol. 120, pp. 1201-1233.

[12] Culley, J.L.B., Larson, W.E. (1987). Susceptibility to compression of a clay loam Haplaquoll. *Soil Sci. Soc. Am. J.*, Vol. 51, pp. 562-567.

[13] Alvarado, G. and Coop, M.R. (2011). On the performance of bender elements in triaxial tests. *Géotechnique*, Vol. 62, No. 1, pp. 1-17.

[14] Jardine, R.J., Fourie, A., Maswoswe, J. and Burland, J.B. (1985). Field and laboratory measurement of soils stiffness. *Proc. 11th Int. Conf. in Soil Mech. and Found. Engin.*, San Francisco, Vol. 2, pp. 511-514.

[15] Viana da Fonseca, A., Matos Fernandes, M., Silva Cardoso, A. (1997). Interpretation of a footing load test n a saprolitic soil from granite. *Géotechnique*. Vol. 47, No. 3, pp. 633-651.

[16] Viana da Fonseca, A., Carvalho, J., Ferreira, C., Santos, J. A., Almeida, F., Pereira, E., Feliciano, J., Grade, J., Oliveira, A. (2006). Characterization of a profile of residual soil from granite combining geological, geophysical, and mechanical testing techniques. *Geotech. & Geolog. Engin.*, Vol. 24, pp. 1307-1348.

[17] Lings, M.L. and Greening, P.D. (2001). A novel bender/extender element for soil testing. *Géotechnique*, Vol. 51, No. 8, pp. 713-717.

[18] Germaine, J.T., Ladd, C.C. (1988). Triaxial testing of saturated cohesive soils. ASTM Spec. Tech. Pub., No. 977, pp. 421-459.

[19] Nocilla, A.M.R.; Coop, M., Colleselli, F. (2006). The mechanics of an Italian silt; an example of "transitional" behaviour. *Géotechnique*, Vol. 56. No. 4, pp. 261-271.

[20] Martins, F.B., Bressani, L.A., Coop, M.R., & Bica, A. (2001). Some aspects of the compressibility behaviour of a clayey sand. *Can. Geotech. J.*, Vol. 38, pp. 1177-1186.

[21] Carrera, A., Coop, M.R., Lancellota, R. (2011). Influence of grading on the mechanical behaviour of Stava tailings. *Géotechnique*, Vol. 61, No. 11, pp. 935-946.

[22] Yamamuro, J.A., Lade, P.V. (1996). Drained sand behavior in axisymmetric tests at high pressures. *J. of Geotech. Engin.*, Vol. 122, No. 2, pp. 109-119.

[23] Shirley, D.J. and Hampton, L.D. (1978). Shear-wave measurements in laboratory sediments. *J. Acoust. Soc. Am.*, Vol. 63, No. 2, pp. 607-613.

[24] Arroyo, M., Muir Wood, D., Greening, P.D., Medina, L., Rio, J. (2006). Effects of sample size on bender-based axial G0 measurements. *Géotechnique*, Vol. 56, No. 1, pp. 39-52.

[25] Vilhar, G., Jovičić, V. (2009). Measurement and interpretation of the small strain stiffness of boštanj silty sand. *Acta Geotechnica Slovenica*, Vol. 6, No. 2, pp. 57-75.

[26] Viana da Fonseca, A., Ferreira, C., Fahey, M. (2009). A framework interpreting bender element tests, combining time-domain and frequency-domain methods. *Geotech. Test. J.*, Vol. 32, No. 2, pp. 1-17.

[27] Amaral, M.F., Viana da Fonseca, A., Arroyo, M., Cascante, G., Carvalho, J., 2011. Compression and shear wave propagation in cemented-sand specimens. *Géotechnique Lett.*, Vol. 1, No. 3, pp. 79-84.

[28] Amaral, M.F., Viana da Fonseca, A., Carvalho, J., Consoli, N.C. (2011). Dynamic Poisson ratio analysis. *Proc. 15th Eur. Conf. on Soil Mech. & Geotech. Engin.*, Vol. 0, pp. 115-120.

[29] Richart, F.E., Hall, J.R., Woods, R.D. (1970). Vibrations of soils and foundations. Prentice-Hall, Inc., Englewood Cliffs, NJ.

[30] Tallavó, F., Cascante, G., Pandey, M. D. (2010). New Methodology for Source Characterization in Pulse Velocity Testing. *Geotech. Test. J.*, Vol. 32, No. 6, pp. 1-16.

[31] Khan, Z., Cascante, G., and El-Naggar, H. (2011). Dynamic properties of cemented sands using the ultrasonic waves. *Can. Geotech. J.*, Vol. 48, pp. 1-15.

[32] Dolinar, B. (2004). Undrained shear strength of saturated cohesive soils depending on consolidation pressure and mineralogical properties. *Acta Geotechnica Slovenica*, Vol. 2, pp. 5-9.